


A cosmological distance measure using radio-loud quasars

L. Huang ^{1,3}*, Z. X. Chang²

¹College of Science, Jiujiang University, Jiujiang 332000, People's Republic of China.

²College of Mathematical and Physical Sciences, HanDan University, Handan 056000, People's Republic of China.

³Key Laboratory of Functional Microscale Materials in Jiangxi Province, Jiujiang 332000, People's Republic of China.

Accepted —. Received —; in original form —

ABSTRACT

We use the X-ray luminosity relation of radio-loud quasars (RLQs) to measure these luminosity distances as well as estimate cosmological parameters. We adopt four parametric models of X-ray luminosity to test luminosity correlation for RLQs and radio-intermediate quasars (RIQs) and give these cosmological distances. By Bayesian information criterion (BIC), the data suggest that the luminosity relation $L_X \propto L_{UV}^{\gamma_{uv}} L_{Radio}^{\gamma_{radio}}$ for RLQs has better goodness of fit, relative to other models, which can be interpreted as this relation being preferred for RLQs. Meanwhile, we compare the results from flat-spectrum radio-loud quasars (FSRLQs) and steep-spectrum radio-loud quasars (SSRLQs), which indicate that their luminosity correlations are not exactly the same. We also consider dividing the RLQs sample into various redshift bins, which can be used to check if the X-ray luminosity relation depends on the redshift. Finally, we apply a combination of RLQs and SNIa Pantheon to verify the nature of dark energy concerning whether or not its density deviates from the constant, and give the statistical results.

Key words: quasars: general–galaxies: high-redshift–cosmology: observations–cosmology: distance scale–cosmology: dark energy

1 INTRODUCTION

With the rapid development of the economy and astronomical technologies, more and more observational data can be used for cosmological distance measurement. Such as SNe Ia (Riess et al. 1998; Amanullah et al. 2010; Betoule et al. 2014; Scolnic et al. 2018), quasars (Risaliti et al. 2015), GRB (Khadka et al. 2021), gravitational wave (Chen et al. 2018; Fu et al. 2019) and so on (Jimenez et al. 2003). On the other hand, these data can also be applied for the test of the Cosmological Principle (Secrest et al. 2021). We consider using radio-loud quasars (RLQs) with luminosity correlation to measure these cosmological luminosity distances.

Radio-loud quasars are one type of quasars, which are categorized by their radio luminosity. Since the discovery of quasars, it has been known that some of them have strong radio emissions and others do not. Strittmatter et al. (1980) showed that a dichotomy can be used in the distribution of the radio luminosity of quasars, Kellermann et al. (1989) also defined different quasars based on the ratio of monochromatic luminosities. RLQs are often defined by a radio-loudness parameter satisfying $\log R > 1$ for the subset of quasars, where R is the ratio of monochromatic luminosities (with units of $\text{erg s}^{-1} \text{Hz}^{-1}$) measured at (rest-frame) 5 GHz and 2500 Å (Stoche et al. 1992; Kellermann et al. 1994). Radio-quiet quasars (RQs) must minimally satisfy $\log R < 1$ and often are found to have $\log R < 0$. This is the traditional division for quasars. The physical reason for the difference between RLQs and RQs populations

remains elusive, several explanations involve the physical origin of radio emission (Laor et al. 2008; Panessa et al. 2019), black hole masses (Lacy et al. 2001), accretion rates (Sikora et al. 2007), and/or spins (Garofalo et al. 2010), which results that a universal function such as the traditional division may not be interpreted by the exact same physical mechanism (Balokovic et al. 2012), but such classical dichotomy is still relevant.

The X-ray properties of RLQs are different from those of RQs. RLQs are generally more X-ray luminous than RQs of matched optical/UV luminosity (Willott et al. 2001; Laor 2000; Meier 2001; Metcalf et al. 2006; Shankar et al. 2010; Garofalo et al. 2010; Browne et al. 1987; Worrall et al. 1987). The X-ray luminosity in RLQs may be correlated with optical/UV and radio luminosity, which can be verified by parameterization methods (Tananbaum et al. 1983; Worrall et al. 1987; Miller et al. 2010; Zhu et al. 2020; Browne et al. 1987). The luminosity correlation might indicate that X-ray emission is not merely created by Compton upscattering of disk photons occurring in a hot “corona”, but also powered directly or indirectly by the radio jet (Evans et al. 2006; Hardcastle et al. 2009; Miller et al. 2010), which makes RLQs regarded as standard candles and can be used for cosmological distance measurement.

Hence, we combine the parameterized model of X-ray luminosity with X-ray, optical/UV, and radio flux at (rest-frame) 5 GHz, 2500 Å, and 2keV to test luminosity correlation as well as obtain luminosity distance. On the other hand, Flat-spectrum radio-loud quasars (FSRLQs) and steep-spectrum radio-loud quasars (SSRLQs) are the two categories of RLQs (Urry et al. 1995; Barthel 1989; Padovani et al. 1992), which can be defined by $\alpha_r > -0.5$ for FSRLQs, and

* E-mail: huanglong20122021@163.com

$\alpha_r \leq -0.5$ for SSRLQs. FSRQs and SSRQs might involve different mechanisms which can be used to explain their X-ray data. Therefore, we consider applying various models to FSRLQs and FSRQs and seek optimal models.

In addition, Worrall et al have used RLQs to check whether luminosity correlations are redshift dependent (Miller et al. 2010). Hence, we also consider dividing the RLQs sample into various redshift bins, which can be used to constrain model parameters and examine whether or not luminosity relations depend on redshift.

In Section 2 of this paper, we introduce the source of data used, including the flux of RLQs and RIQs in the radio, optical/UV, and X-ray wavebands. In Section 3, we employ four parametric models to test the X-ray luminosity correlation of RLQs and RIQs, which include X-ray luminosity as a sole function of optical/UV luminosity and as a joint function of optical/UV and radio luminosity. In Section 4, we compare and analyze four different models by using the Bayesian information criterion (BIC), meanwhile obtaining cosmological luminosity distance. Furthermore, we consider dividing the RLQs sample into various redshift bins, which can be used for checking if the X-ray luminosity relation depends on the redshift. In Section 5, we apply a combination of RLQs and SNIa Pantheon to reconstruct the dark energy equation of state $w(z)$, which can be used to test the nature of dark energy concerning whether or not its density deviates from the constant. In Section 6, we summary the paper.

2 DATA USED

Radio (e.g., Faint Images of the Radio Sky) surveys (Helfand et al. 2015), modern optical (e.g., Sloan Digital Sky Survey) (Lyke et al. 2020; Paris et al. 2018; Alam et al. 2015; Richards et al. 2002), and archival X-ray data from Chandra (Evans et al. 2010), XMM-Newton (Traulsen et al. 2019), and ROSAT (Sun et al. 2012) provide large amount of quasars data, which can be used to investigate luminosity correlation for quasars. Miller et al. (2010) obtained 654 sample including RIQs and RLQs, which are selected from SDSS/FIRST observations and high quality X-ray coverage from Chandra, XMM-Newton, or ROSAT (Suchkov et al. 2006; Jester et al. 2006; Green et al. 2009; Young et al. 2017; Schneider et al. 2017; Richards et al. 2009). Zhu et al. (2020) further selected new RLQs using the Sloan Digital Sky Survey, and the radio data are from the Faint Images of the Radio Sky at Twenty-Centimeters, and the NRAO VLA Sky Survey (Helfand et al. 2015; Paris et al. 2017; Banfield et al. 2015; York et al. 2000; Becker et al. 1995; Condon et al. 1998). The X-ray luminosities can be obtained from Chandra and XMM Newton observations (Evans et al. 2010; Rosen et al. 2016).

Therefore, we consider to use a combined data from Miller et al. (2010) and Zhu et al. (2020). The observed 1.4GHz flux is utilized to calculate rest-frame radio flux at 5GHz (F_{radio}) by assuming $\alpha_r = -0.5$. In the same way, the i-band apparent magnitude (m_i) can be used for calculating rest-frame optical/UV flux at 2500 Å (F_{UV}), where an optical spectral index of $\alpha_o = -0.5$ are assumed for the K-correction (Richards et al. 2006). Count rates were also converted to the unabsorbed flux density at observed-frame 2keV using PIMMs, where a specifying Galactic column density and a power-law spectrum $\Gamma = 1.5$ are considered (Miller et al. 2010), which can be used to determine bandpass-corrected rest-frame 2 keV flux.

Meanwhile, a part of RIQs and RLQs from FIRST measured flux densities at 1.4GHz can not directly obtain their radio slopes, Zhu et al. (2020) matched those quasars with other radio surveys, the

latter can provide radio fluxes at another wavelength, which can be applied to calculate radio slopes. Other radio surveys include the Green Bank 6-cm (GB6) Radio Source Catalog at 4.85GHz (Gregory et al. 1996), Westerbork Northern Sky Survey at 325MHz (Rengelink et al. 1997), TGSS Alternative Data Release at 150MHz (Intema et al. 2017), LoTSS DR1 at 144MHz (Shimwell et al. 2019), and the Very Large Array Sky Survey (VLASS) at 3GHz (Hancock et al. 2012, 2018). Zhu et al. (2020) also gather their multi-band radio flux densities from the NED¹ or VizieR For RLQs that are not matched with those radio surveys.

In this paper, we only consider RLQs with $\log R > 2$, and RIQs satisfy $1 \leq \log R \leq 2$. Meanwhile, FSRLQs are given by $\alpha_r > -0.5$, and SSRLQs have $\alpha_r \leq -0.5$. We adopt parametric methods to test their luminosity correlation.

3 PARAMETERIZING THE X-RAY LUMINOSITY OF RLQS AND RIQS

We use different parameterization methods to test luminosity correlation, which involve different physical mechanisms. The most common form is (Tananbaum et al. 1983; Worrall et al. 1987; Miller et al. 2010; Zhu et al. 2020)

$$\begin{aligned} & \text{Model} \\ I : \log L_X &= \alpha + \gamma_{uv} \log L_{UV} + \gamma'_{radio} \log L_{Radio}, \end{aligned} \quad (1)$$

The above equation can become the relation $L_X \propto L_{UV}^{\gamma_{uv}} L_{Radio}^{\gamma'_{radio}}$. Using formula $L = 4\pi D_L^2 F$ in it, we get

$$\begin{aligned} \log F_X &= \Phi(F_{UV}, F_{radio}, D_L) \\ &= \alpha + \gamma_{uv} \log F_{UV} + \gamma'_{radio} \log F_{radio} \\ &\quad + (\gamma_{uv} + \gamma'_{radio} - 1) \log(4\pi D_L^2), \end{aligned} \quad (2)$$

where F_X , F_{UV} and F_{radio} are measured at (rest-frame) 2keV, 2500 Å and 5GHz, D_L is the luminosity distance, which can be calculated by integral formula of $D_L - z$ relation. Thus equation (2) can be used to test X-ray luminosity correlation for RLQs and RIQs.

We can also consider other models, including (Miller et al. 2010; Zhu et al. 2020; Browne et al. 1987)

$$II : \log L_X = \log(AL_{UV}^{\gamma_{uv}} + BL_{Radio}^{\gamma_{radio}}), \quad (3)$$

$$III : \log L_X = \log(AL_{UV}^{\gamma_{uv}} L_{Radio}^{\gamma'_{radio}} + BL_{Radio}^{\gamma_{radio}}), \quad (4)$$

Model II and Model III can become the relation $L_X = AL_{UV}^{\gamma_{uv}} + BL_{Radio}^{\gamma_{radio}}$ and $L_X = AL_{UV}^{\gamma_{uv}} L_{Radio}^{\gamma'_{radio}} + BL_{Radio}^{\gamma_{radio}}$. The above three models concern that X-ray luminosity is related to both optical/UV luminosity and radio luminosity. The last model is considered that X-ray luminosity is only correlated with optical/UV luminosity, and its parametric form is (Miller et al. 2010; Bisogni et al. 2021)

$$IV : \log L_X = \alpha + \gamma_{uv} \log L_{UV}, \quad (5)$$

Similarly, from Equations (3),(4) and (5), we can get X-ray flux F_X as the function of F_{UV} , F_{radio} and D_L , which can be used to verify X-ray luminosity relation.

¹ <http://nedwww.ipac.caltech.edu/>

4 MODELS CONSTRAINS FROM RLQS AND RIQS

4.1 Fitting the Models to RLQs and RIQs

We fit parametric models by minimizing a likelihood function consisting of a modified χ^2 function based on MCMC, allowing for an intrinsic dispersion σ (Risaliti et al. 2015)

$$-2 \ln L = \sum_{i=1}^N \left\{ \frac{[\log(F_X)_i - \Phi(F_{UV}, F_{radio}, D_L)_i]^2}{s_i^2} + \ln(2\pi s_i^2) \right\}, \quad (6)$$

where $\Phi(F_{UV}, F_{radio}, D_L)$ is given by equation (2), and $s_i = \sigma$, σ is the intrinsic dispersion, which can be fitted as a free parameter. Also, σ is much larger than measurement error in most cases.

The parameters α and Hubble constant H_0 are degenerate when fitting equation (2), we fix $H_0 = 70 \text{ km s}^{-1} \text{ Mpc}^{-1}$ (Reid et al. 2019; Aghanim et al. 2020). If we want to better test X-ray luminosity relation and further seek optimal model, we should not fix Ω_m . Therefore, we fit four models to RIQs and RLQs without fixing Ω_m , and select best model.

Meanwhile, we measure the distance modulus for FSRLQs and SSRLQs. For Model I, Equation (2) gives distance modulus as

$$DM = \frac{5[\log F_X - \gamma_{uv} \log F_{UV} - \gamma'_{radio} F_{radio} - \alpha']}{2(\gamma_{uv} + \gamma'_{radio} - 1)}, \quad (7)$$

where $\alpha' = \alpha + (\gamma_{uv} + \gamma'_{radio} - 1) \log(4\pi)$. The error is

$$\sigma_{DM} = \frac{5\sigma}{2(\gamma_{uv} + \gamma'_{radio} - 1)}. \quad (8)$$

In the same way, for model IV, the distance modulus is

$$DM = \frac{5[\log F_X - \gamma_{uv} \log F_{UV} - \alpha']}{2(\gamma_{uv} - 1)}. \quad (9)$$

and its error

$$\sigma_{DM} = \frac{5\sigma}{2(\gamma_{uv} - 1)}, \quad (10)$$

For Model II and Model III, distance modulus can be calculated by numerical solution of equations (3) and (4).

We adopt maximum likelihood function (equation (6)) based on MCMC to constrain four models, the fit results are shown in table 1. Meanwhile, we compare FSRLQs and SSRLQs distance modulus from model I and model IV, which are shown in fig 1. Fig 2 shows FSRLQs and SSRLQs distance modulus from a fit of Model I when assuming Λ CDM cosmology, and their averages in small redshift bins.

4.2 Models analysis and comparison

We use BIC to seek an optimal model. The BIC is

$$BIC = -2 \ln L_{\max} + k \ln N, \quad (11)$$

where L_{\max} is the maximum likelihood, k is the number of free parameters of the model, and N is the number of data points.

By comparing BIC in table 1 from fitting for different models to RIQs, we find Model IV has the smallest BIC, which might indicate that the X-ray luminosity of RIQs is not strongly correlated with their radio luminosity. As for RLQs, BIC for Model I, Model II, and Model III are far smaller than Model IV, which implies X-ray luminosity of RLQs is not only connected with optical/UV luminosity but also related to radio luminosity. Moreover, distance modulus for RLQs including FSRLQs and SSRLQs obtained from Model I have smaller dispersion (see fig 1), relative to Model IV. Meanwhile, for RLQs,

the BIC of Model I is less than Model II and Model III, which shows that the luminosity relation $L_X \propto L_{UV}^{\gamma_{uv}} L_{Radio}^{\gamma'_{radio}}$ for RLQs has some superiority, relative to other models. A possible reason for the luminosity correlations in RLQs is that a fraction of the nuclear X-ray emission is directly or indirectly powered by the radio jet (Hardcastle et al. 2009; Miller et al. 2010), the specific physical mechanism needs to be further understood.

Furthermore, for the fitting results BIC, there is a difference between FSRLQs and SSRLQs for Model I. The goodness of fit for SSRLQs seems to be better, which implies FSRLQs probably involve more physical processes (Landt et al. 2006; Zhu et al. 2020).

4.3 Analysis of the relation $L_X \propto L_{UV}^{\gamma_{uv}} L_{Radio}^{\gamma'_{radio}}$

We divide the RLQs data in several redshift bins, which can be used to check if luminosity relation $L_X \propto L_{UV}^{\gamma_{uv}} L_{Radio}^{\gamma'_{radio}}$ depend on redshift. The redshift bins satisfy $\Delta \log z = 0.1$. We adopt parametric model (Risaliti et al. 2015)

$$\log F_X = \alpha(z) + \gamma_{uv}(z) \log F_{UV} + \gamma'_{radio}(z) \log F_{radio}, \quad (12)$$

where $\alpha(z)$, $\gamma_{uv}(z)$, $\gamma'_{radio}(z)$ are free parameters. We apply segmented RLQs data to fit $\gamma_{uv}(z)$ and $\gamma'_{radio}(z)$ as well as test whether there are a dependency upon redshift. The fit results of $\gamma_{UV}(z)$, $\gamma'_{radio}(z)$, $\sigma(z)$ at different redshift are illustrated in fig 3, it is easy to see that their value do not obviously deviate from the average, which shows there are no obvious evidence for any significant redshift evolution. The average values of parameters are $\langle \gamma_{uv} \rangle = 0.49 \pm 0.165$, $\langle \gamma'_{radio} \rangle = 0.248 \pm 0.083$.

5 THE RECONSTRUCTION OF DARK ENERGY EQUATION OF STATE $w(z)$

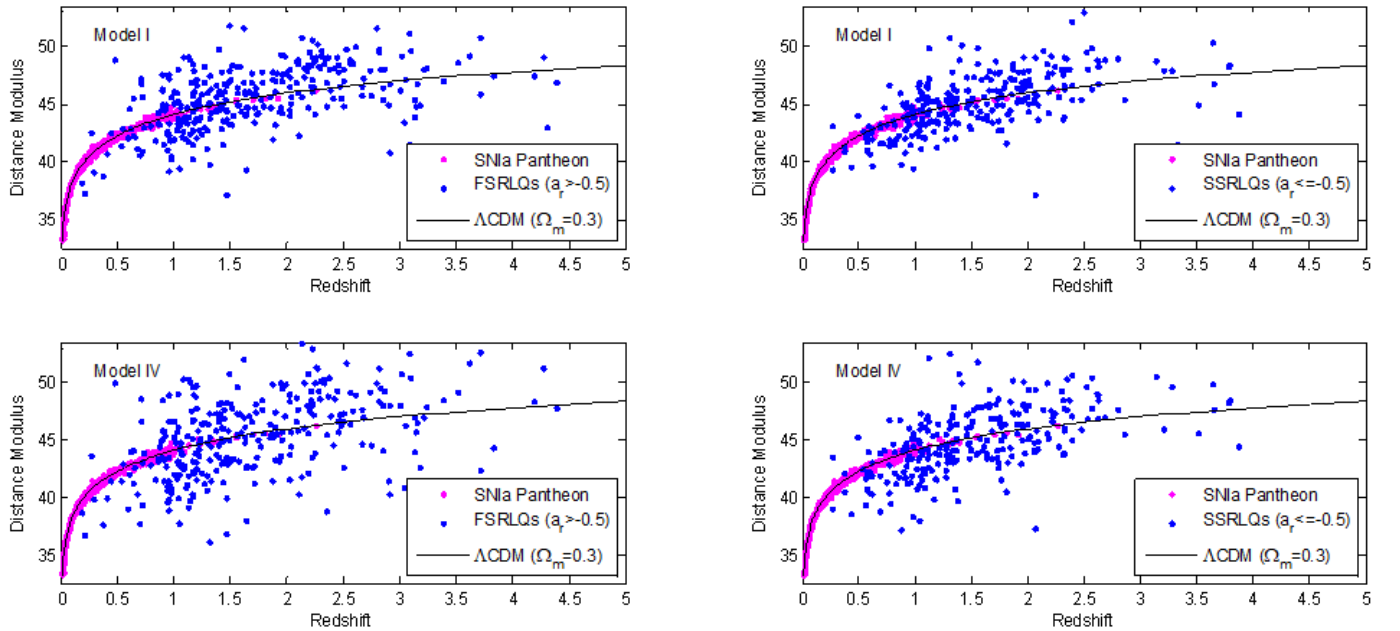
Although cosmological constant Λ CDM model can be used to effectively explain the accelerating expansion of universe and the cosmic microwave background (CMB) anisotropies (Riess et al. 1998; Amanullah et al. 2010; Betoule et al. 2014; Scolnic et al. 2018; Conley et al. 2010; Aghanim et al. 2020; Hu et al. 2002; Spergel et al. 2003; Ade et al. 2016; Aghanim et al. 2016), the origin and nature of dark energy density and pressure are still unclear.

Dark energy can be studied using two main approaches. The first is to constrain dark energy physical models and attempt to explain the physical origin of its density and pressure (Peebles et al. 2003; Ratra et al. 1988; Li 2004; Mazishvili et al. 2007; Amendola et al. 2000; Huang et al. 2021; Gao et al. 2020). Understanding the physical nature of dark energy is important for our universe. Whether or not the dark energy is composed of Fermion pairs in a vacuum or Boson pairs, Higgs field, and whether it has weak isospin, which may determine whether it can be observed by experiment. The second is to focus on the properties of dark energy, investigating whether or not its density evolves with time, this can be checked by reconstructing the dark energy equation of state $w(z)$ (Linder 2003; Maor et al. 2002), which is independent of physical models. The high redshift observational data can better solve these issues.

The reconstruction of the equation of state includes parametric and non-parametric methods (Huterer et al. 2003; Clarkson et al. 2010; Holsclaw et al. 2010; Seikel et al. 2012; Shafieloo et al. 2012; Crittenden et al. 2009, 2012; Zhao et al. 2012; Huang et al. 2021). We use RLQs and SNIa to reconstruct $w(z)$ by parametric method assuming X-ray luminosity relation Equation (2), which can be used for testing the nature of dark energy.

Table 1. Model fitting results for RIQs and RLQs

Model	Sample	α	A	γ_{uv}	B	γ_{radio}	γ'_{radio}	σ	Ω_m	$-2\ln L_{max}/N$
I	RIQs	4.99 ± 0.67	–	0.454 ± 0.016	–	–	0.245 ± 0.01	0.369 ± 0.02	0.162 ± 0.042	119/144
	FSRLQs	5.24 ± 0.31	–	0.383 ± 0.007	–	–	0.301 ± 0.009	0.282 ± 0.012	0.09 ± 0.013	95/305
	SSRLQs	6.07 ± 0.232	–	0.4 ± 0.012	–	–	0.259 ± 0.008	0.261 ± 0.01	0.136 ± 0.075	32/266
	RLQs	5.29 ± 0.108	–	0.416 ± 0.006	–	–	0.27 ± 0.006	0.276 ± 0.008	0.088 ± 0.037	147/571
	RLQs+RIQs	5.33 ± 0.176	–	0.456 ± 0.007	–	–	0.231 ± 0.004	0.298 ± 0.009	0.175 ± 0.029	290/715
II	RIQs	–	6.69 ± 0.546	0.65 ± 0.019	6 ± 0.338	0.626 ± 0.007	–	0.371 ± 0.024	0.2 ± 0.07	118/144
	FSRLQs	–	5.93 ± 0.284	0.68 ± 0.009	4.37 ± 0.282	0.66 ± 0.008	–	0.29 ± 0.012	0.11 ± 0.063	97/305
	SSRLQs	–	5.51 ± 0.154	0.7 ± 0.005	6.06 ± 0.188	0.61 ± 0.005	–	0.26 ± 0.012	0.069 ± 0.109	35/266
	RLQs	–	5.71 ± 0.18	0.69 ± 0.006	6 ± 0.207	0.61 ± 0.005	–	0.278 ± 0.008	0.084 ± 0.083	155/571
	RLQs+RIQs	–	5.99 ± 0.146	0.6 ± 0.005	6.02 ± 0.09	0.61 ± 0.002	–	0.3 ± 0.007	0.22 ± 0.09	302/715
III	RIQs	–	7.14 ± 0.557	0.39 ± 0.021	3.76 ± 0.3	0.65(fixed)	0.235 ± 0.008	0.375 ± 0.023	0.44 ± 0.08	118/144
	FSRLQs	–	4.62 ± 0.322	0.43 ± 0.014	2.65 ± 0.312	0.65(fixed)	0.276 ± 0.014	0.28 ± 0.011	0.085 ± 0.03	94/305
	SSRLQs	–	6.26 ± 0.292	0.42 ± 0.01	3.38 ± 0.353	0.65(fixed)	0.23 ± 0.012	0.26 ± 0.011	0.105 ± 0.05	32/266
	RLQs	–	5.45 ± 0.373	0.43 ± 0.007	2.53 ± 0.637	0.65(fixed)	0.25 ± 0.008	0.276 ± 0.007	0.062 ± 0.034	145/571
	RLQs+RIQs	–	5.43 ± 0.275	0.46 ± 0.006	3.28 ± 0.393	0.65(fixed)	0.225 ± 0.008	0.3 ± 0.008	0.1 ± 0.027	289/715
IV	RIQs	5.78 ± 0.225	–	0.687 ± 0.0076	–	–	–	0.37 ± 0.02	0.35 ± 0.088	120/144
	FSRLQs	4.38 ± 0.351	–	0.741 ± 0.012	–	–	–	0.316 ± 0.012	0.06 ± 0.034	158/305
	SSRLQs	5.47 ± 0.311	–	0.703 ± 0.01	–	–	–	0.289 ± 0.012	0.056 ± 0.041	79/266
	RLQs	5.96 ± 0.32	–	0.704 ± 0.01	–	–	–	0.3 ± 0.009	0.06 ± 0.027	248/571
	RLQs+RIQs	5.71 ± 0.247	–	0.695 ± 0.008	–	–	–	0.33 ± 0.008	0.226 ± 0.037	440/715

**Figure 1.** Distance modulus from fitting Model I and Model IV with a prior flat Λ CDM model to FSRLQs and SSRLQs. Blue points are FSRLQs and SSRLQs distance modulus, pink points are SN Ia from Pantheon sample. The blue line shows a flat Λ CDM model fit with $\Omega_m = 0.3$.**Table 2.** Fit results on model parameters for a combination of SN Ia and RLQs

	Sample	α	γ_{uv}	γ'_{radio}	σ	Ω_m	w_0	w_α	χ^2_{Total}/N
Λ CDM	SN + RLQs	6.28 ± 0.259	0.43 ± 0.007	0.225 ± 0.01	0.278 ± 0.007	0.275 ± 0.007	–	–	1151.1/1619
	SN + FSRLQs	4.13 ± 0.526	0.475 ± 0.014	0.25 ± 0.013	0.285 ± 0.012	0.276 ± 0.007	–	–	1097/1353
	SN + SSRLQs	6.57 ± 0.406	0.4 ± 0.012	0.24 ± 0.008	0.26 ± 0.012	0.275 ± 0.008	–	–	1036.8/1314
$w_0 w_\alpha$ CDM	SN + RLQs	5.42 ± 0.259	0.45 ± 0.009	0.23 ± 0.006	0.28 ± 0.008	0.33 ± 0.0017	-1.168 ± 0.047	0.232 ± 0.517	1147.7/1619
	SN + FSRLQs	5.35 ± 0.17	0.41 ± 0.014	0.274 ± 0.011	0.286 ± 0.011	0.3136 ± 0.035	-1.158 ± 0.062	0.578 ± 0.478	1091.3/1353
	SN + SSRLQs	6.8 ± 0.463	0.42 ± 0.01	0.215 ± 0.0018	0.26 ± 0.012	0.29 ± 0.033	-1.11 ± 0.07	0.63 ± 0.358	1032/1314

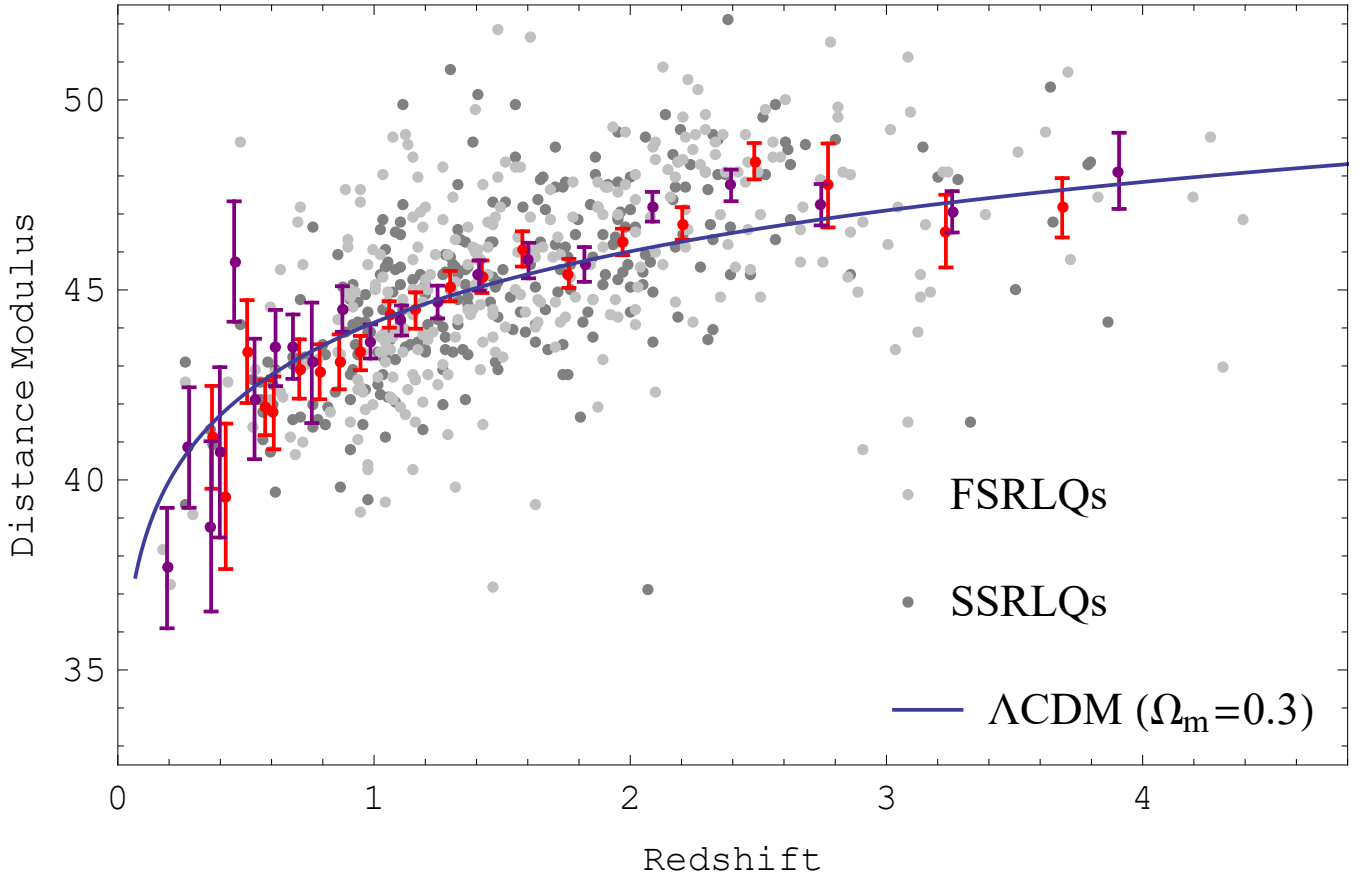


Figure 2. FSRLQs (light grey points) and SSRLQs distance modulus (grey points) from a fit of Model I when assuming Λ CDM cosmology. The purple and red points are FSRLQs and SSRLQs averages in small redshift bins. The blue line shows a flat Λ CDM model fit with $\Omega_m = 0.3$.

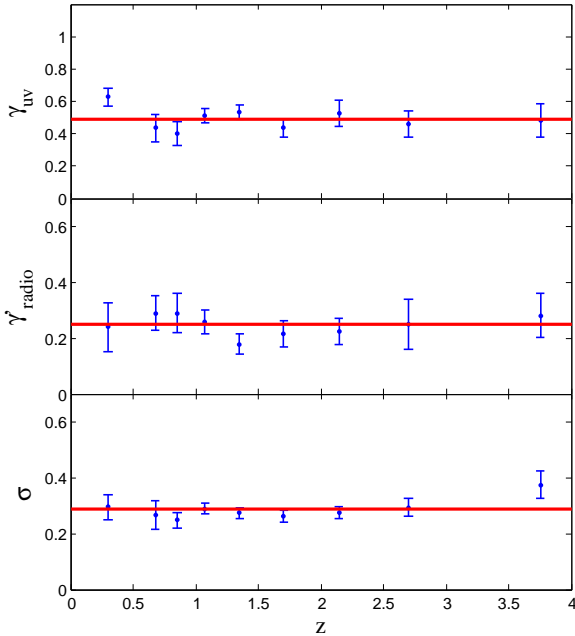


Figure 3. $F_X - F_{UV}/F_{radio}$ correlation in narrow redshift intervals. Blue points are the fit results of $\gamma_{UV}(z)$, $\gamma_{radio}(z)$, $\sigma(z)$ at different redshift. The horizontal lines show their average values.

SN Ia Pantheon sample is the combination of SNIa from the Pan-STARRS1 (PS1), the Sloan Digital Sky Survey (SDSS), SNLS, and various low- z and Hubble Space Telescope samples. There are 279 SNIa provided by PS1 (Scolnic et al. 2018), and SDSS presented 335 SNIa (Betoule et al. 2014; Gunn et al. 2006, 1998; Sako et al. 2007, 2014). The rest of Pantheon sample are from the CfA1 – 4, CSP, and Hubble Space Telescope (HST) SN surveys (Amanullah et al. 2010; Conley et al. 2010). This extended sample of 1048 SNIa is called the Pantheon sample.

The integral formula of $D_L - z$ relation in flat space can be written as

$$D_L = \frac{1+z}{H_0} \int_0^z dz' [\Omega_m(1+z')^3 + \Omega_R(1+z')^4 + \Omega_{DE}^{(0)} e^{\int_0^{z'} \frac{1+w(z'')}{1+z''} dz''}]^{-1/2} \quad (13)$$

where Ω_R is radiation density. $\Omega_{DE}^{(0)}$ is the present dark energy density and satisfies $\Omega_{DE}^{(0)} = 1 - \Omega_m$ when ignoring Ω_R , $w(z)$ is dark energy equation of state. We choose parametric form for $w(z)$

$$w(z) = w_0 + w_a \frac{z}{1+z}. \quad (14)$$

Therefore dark energy density is

$$\Omega_{DE}(z) = \Omega_{DE}^{(0)} (1+z)^{3(1+w_0+w_a)} \exp[-3w_a z/(1+z)]. \quad (15)$$

We constrain $w_0 w_a$ CDM model parameters for RLQs and SNIa by minimizing χ_{Total}^2 , the χ_{Total}^2 is

$$\chi_{Total}^2 = -2 \ln L^{RLQs} + \chi_{SN}^2, \quad (16)$$

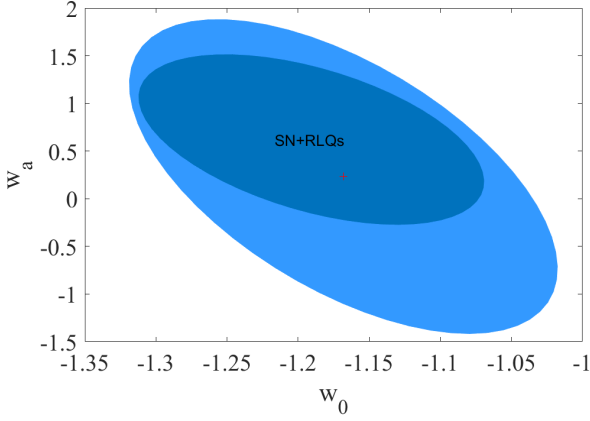


Figure 4. 68% and 95% contours for w_0 and w_a from a fit of the X-ray luminosity relation $L_X \propto L_{UV}^{\gamma_{uv}} L_{Radio}^{\gamma_{radio}}$ with Λ CDM and $w_0 w_a$ CDM model to a combination of SNIa and RLQs. The + dot in responding color represents the best fitting values for w_0 , w_a .

where $-2 \ln L^{RLQs}$ is given by equation (6), and χ_{SN}^2 can be expressed as

$$\chi_{SN}^2 = \Delta\mu^T C_{\mu_{ob}}^{-1} \Delta\mu, \quad (17)$$

where $\Delta\mu = \mu - \mu_{th}$. C_{μ} is the covariance matrix of the distance modulus μ .

We use equation (16) to fit model parameters, and fit results are shown in table 2, the results shows $w_0 w_a$ CDM has better goodness of fit than Λ CDM, and $\Delta\chi_{Total}^2$ is improved by -3.4 , which indicate Λ CDM model is in tension with RLQs at $\sim 1.5\sigma$. Meanwhile fig 4 illustrates 68% and 95% contours for w_0 and w_a from a combination of SNIa and RLQs, assuming the X-ray luminosity relation $L_X \propto L_{UV}^{\gamma_{uv}} L_{Radio}^{\gamma_{radio}}$. The distance modulus and properties of the 571 RLQs are listed in Table 3 (the full data can be downloaded from [MNRAS](#) or [J/MNRAS/515/1358](#)).

6 SUMMARY

The verification of X-ray luminosity correlation for RIQs and RLQs could make us understand more of their physical mechanism. We obtain a sample of 144 RIQs and 571 RLQs with radio, optical/UV, and X-ray coverage. Firstly, we adopt four parametric methods to test the correlation between X-ray, optical/UV, and radio luminosity. Data suggest that X-ray luminosity relation $L_X \propto L_{UV}^{\gamma_{uv}} L_{Radio}^{\gamma_{radio}}$ is more suitable for RLQs by comparing BIC, which implies X-ray luminosity of RLQs are not only related to optical/UV luminosity but also connected with radio luminosity. Similarly, X-ray luminosity relation $L_X \propto L_{UV}^{\gamma_{uv}}$ is preferred by RIQs, which indicates that the X-ray luminosity of RIQs is not strongly correlated with their radio luminosity. Meanwhile, we compare the results from FSRLQs and SSRLQs using a fit of X-ray luminosity relation $L_X \propto L_{UV}^{\gamma_{uv}} L_{Radio}^{\gamma_{radio}}$, the goodness of fit for SSRLQs seems to be better, which indicates that X-ray luminosity $L_X \propto L_{UV}^{\gamma_{uv}} L_{Radio}^{\gamma_{radio}}$ is more suitable for SSRLQs compared to FSRLQs.

Secondly, We divide the RLQs data into several redshift bins and combine a special model to check if there is a redshift evolution of X-ray luminosity relation $L_X \propto L_{UV}^{\gamma_{uv}} L_{Radio}^{\gamma_{radio}}$, the fit results show the

model parameters approach to the constant, which implies there is not an obvious redshift evolution for $L_X \propto L_{UV}^{\gamma_{uv}} L_{Radio}^{\gamma_{radio}}$.

Finally, we employ a joint of SNIa and RLQs to reconstruct the dark energy equation of state, which can be used to test the nature of dark energy. the results show $w_0 w_a$ CDM model is superior to cosmological constant Λ CDM model at $\sim 1.5\sigma$.

In the future, we will cross-correlate the SDSS quasar catalogs with the XMM-Newton, Chandra archives, and radio surveys. We expect to obtain several hundred RLQs at high redshift ($z > 3$) with multi-wavelength coverage. The high redshift observational data can better test the properties of dark energy, which will dominate the future of the universe, that the universe continue expanding or change from expansion to contraction. It will similarly determine the future of humanity.

ACKNOWLEDGEMENTS

We thank Dr. Ning Chang for his useful discussion, and suggestions for revision.

DATA AVAILABILITY

The data underlying this article are available in the article and in its online supplementary material.

REFERENCES

- Ade, P. A., Aghanim, N., Arnaud, M., Ashdown, M., et al. 2016, *A&A*, 594, A13.
- Aghanim, N., Ashdown, M., Aumont, J., Baccigalupi, C., et al. 2016, *A&A*, 596, A107.
- Aghanim, N., Akrami, Y., Ashdown, M., Aumont, J., Baccigalupi, C., et al. 2020, *A&A*, 641, A6.
- Amanullah, R., Lidman, C., & Rubin, D., et al. 2010, *APJ*, 716, 712.
- Amendola, L. 2000, *PhRvD*, 62, 043511.
- Alam, S., Albareti, F. D., Prieto, C. A., Anders, F., Anderson, S. F., et al. 2015, *APJS*, 219, 12.
- Banfield, J. K., et al. 2015, *MNRAS*, 453, 2326.
- Balokovic, M., Smolcic, V., Ivezić, Z., et al. 2012, *APJ*, 759, 30.
- Barthel, P. D. 1989, *APJ*, 336, 606.
- Becker, R. H., White, R. L., Helfand D. J. 1995, *APJ*, 450, 559.
- Betoule, M., Kessler, R., & Guy, J., et al. 2014, *A&A*, 568, A22.
- Bisogni, S., Lusso, E., Civano, F., Nardini, E., Risaliti, G., Elvis, M., Fabbiano, G., 2021, arXiv preprint arXiv:2109.03252.
- Browne, I. W. A., & Murphy, D. W. 1987, *MNRAS*, 226, 601.
- Chen, H. Y., Fishbach, M., Holz, D. E. *Nature*, 2018, 562, 545.
- Clarkson, C., Zunckel, C. 2010, *PhRvL*, 104, 211301.
- Condon, J. J., Cotton, W. D., Greisen, E. W., Yin, Q. F., et al. 1998, *AJ*, 115, 1693.
- Conley, A., Guy, J., Sullivan, M., Regnault, N., et al. 2010, *APJS*, 192 1.
- Crittenden, R. G., Pogosian, L., and Zhao, G. B. 2009, *JCAP*, 0912, 025.
- Crittenden, R. G., Zhao, G. B., Pogosian, L., Samushia, L., and Zhang, X. 2012, *JCAP*, 1202, 048.
- Evans, D. A., Worrall, D. M., Hardcastle, M. J., et al. 2006, *APJ*, 642, 96.
- Evans, I. N., Primini, F. A., Glotfelty, K. J., Anderson, C. S., et al. 2010, *APJS*, 189, 37.
- Fu, G. Z., Xing, C. C., and Na, W. 2020, *EPJC*, 80, 1.
- Fu, X., Zhou, L., and Chen, J. 2019, *PhRvD*, 99, 083523.
- Garofalo, D., Evans, D. A., and Sambruna, R. M. 2010, *MNRAS*, 406, 975.
- Green, P. J., et al. 2009, *APJ*, 690, 644.
- Gregory, P. C., Scott, W. K., Douglas, K., Condon, J. J. 1996, *ApJS*, 103, 427.
- Gunn, J.E., et al. 2006, *AJ*, 131, 2332 .
- Gunn, J.E., et al. 1998, *AJ*, 116, 3040.

Table 3. The properties of the 571 RLQs, DM are the distance modulus from a fit of the X-ray luminosity relation $L_X \propto L_{UV}^{\gamma_{UV}} L_{Radio}^{\gamma_{Radio}}$ with Λ CDM model, σ_{DM} are their error.

<i>SDSS name</i>	z	m_i	F_{UV}	F_{radio}	F_X	$\log R$	α_r	DM	σ_{DM}
083946.22+511202.8	4.39	18.98	-23.62	-21.03	-27.43	2.46	0.17	46.19	2.014
091824.38+063653.3	4.192	19.28	-23.75	-21.15	-27.59	2.47	0.25	46.76	2.014
121453.46+300832.7	3.505	19.96	-24.06	-21.51	-27.58	2.43	-0.77	45.12	2.014
080928.21+255240.2	2.853	20.81	-24.33	-21.22	-27.57	2.99	-0.35	44.7	2.014
122012.04+300250.5	1.733	20.13	-24.06	-21.14	-27.29	2.81	-0.64	43.62	2.014

Hancock, P. J., Murphy, T., Gaensler, B. M., Hopkins, A., Curran, J. R. 2012, MNRAS, 422, 1812.

Hancock, P. J., Trott, C. M., Hurley-Walker, N. 2018, PASA, 35, e011.

Hardcastle, M. J., Evans, D. A., Croston, J. H., 2009, MNRAS, 396, 1929.

Helfand, D. J., White, R. L., and Becker, R. H. 2015, APJ, 801, 26.

Holsclaw, T., Alam, U., Sansó, B., et al. 2010, PhRvL, 105, 241302.

Huang, L., Yang, X., and Liu, X. 2021, APJ, 913, 24.

Huang, L., Yang, X., and Liu, X. 2021, Chinese Physics C, 45, 125102.

Huterer, D., Starkman, G. 2003, PhRvL, 90, 031301.

Hu, W., Dodelson, S. 2002, ARA&A, 40, 171.

Intema, H. T., Jagannathan, P., Mooley, K. P., Frail, D. A. 2017, A&A, 598, A78.

Jester, S., Harris, D. E., Marshall, H. L., and Meisenheimer, K. 2006, ApJ, 648,900.

Jimenez, R., Verde, L., Treu, T., et al. 2003, APJ, 593, 622.

Kellermann, K. I., Sramek, R. A., Schmidt, M., Green, R. F., and Shaffer, D. B. 1994, APJ, 108, 1163.

Kellermann, K. I., Sramek, R., Schmidt, M., Shaffer, D. B., &Green, R. 1989, APJ, 98, 1195.

Khadka, N., Luongo, O., Muccino M, et al. 2021, arXiv preprint arXiv:2105.12692.

Lacy, M., Laurent-Muehleisen, S. A., Ridgway, S. E., et al. 2001, APJ, 551, L17.

Landt, H., Perlman, E. S., Padovani, P., 2006, APJ, 637, 183.

Laor, A. 2000, APJ, 543, L111.

Laor, A., Behar, E., 2008, MNRAS, 390, 847.

Linder, E. V. 2003, PhRvL, 90, 091301.

Li, M. 2004, Phys. Lett. B, 603, 1.

Lyke, B. W., Higley, A. N., McLane, J. N., Schurhammer, D. P., et al. 2020, APJS, 250, 8.

Maor, I., Brusteim, R., McMahon, J., and Steinhardt, P. J. 2002, PhRvD, 65, 123003.

Maziashvili, M. 2007, IJMPD, 16, 1531.

Meier, D. L. 2001, APJ, 548, L9.

Metcalf, R. B., &Magliocchetti, M. 2006, MNRAS, 365, 101.

Miller, B. P., Brandt, W. N., Schneider, D. P., Gibson, R. R., Steffen, A. T., and Wu, J. 2010, APJ, 726, 20.

Padovani, P., and Urry, C. M. 1992, APJ, 387, 449.

Panessa, F., Baldi, R. D., Laor, A., et al. 2019, Nature Astronomy, 3, 387.

Paris, I., Petitjean, P., Ross, N. P., Myers, A. D., Aubourg, E., et al. 2017, A&A, 597, A79.

Paris, I., Petitjean, P., Aubourg, E., Myers, A. D., Streblyanska, A., et al. 2018, A&A, 613, A51.

Peebles, P. J. E., Ratra, B. 2003, Rev. Mod. Phys, 75, 559.

Ratra, B., Peebles, P. J. 1988, PhRvD, 37, 3406.

Reid, M. J., Pesce, D. W., Riess, A. G. 2019, ApJL, 886, L27.

Rengelink, R. B., Tang, Y., de Bruyn, A. G., et al. 1997, A&AS, 124, 259.

Richards, G. T., et al. 2006, ApJS, 166, 470.

Richards, G. T., et al. 2009, ApJS, 180, 67.

Richards, G. T., Fan, X., Newberg, H. J., Strauss, M. A., Berk, D. E. V., et al. 2002, APJ, 123, 2945.

Riess, et al. 1998, AJ, 116, 1009.

Risaliti, G., &Lusso, E. 2015, APJ, 815, 33.

Rosen, S. R., Webb, N. A., Watson, M. G., Ballet, J., et al. 2016, A&A, 590, A1.

Sako, K., et al. 2007, AJ, 135, 348.

Sako, L., et al. 2014, PASP, 130, 064002.

Schneider, D. P., et al. 2007, AJ, 134, 102.

Scolnic, D. M., Jones, D. O., &Rest, A., et al. 2018, APJ, 859, 101.

Secrest, N. J., et al. 2021, APJL, 908, L51.

Seikel, M., Clarkson, C., Smith, M., et al. 2012, JCAP, 06, 036.

Shafieloo, A., Kim, A. G., Linder, E. V., et al. 2012, PhRvD, 85, 123530.

Shankar, F., Sivakoff, G. R., Vestergaard, M., and Dai, X. 2010, MNRAS, 401, 1869.

Shimwell T. W., et al. 2019, A&A, 622, A1.

Sikora, M., Stawarz, L., Lasota, J. P., 2007, ApJ, 658, 815.

Spergel, D. N., Verde, L., Peiris, H. V., et al. 2003, APJS, 148, 175.

Stocke, J. T., Morris, S. L., Weymann, R. J., and Foltz, C. B. 1992, APJ, 396, 487.

Strittmatter, P. A., Hill, P., Pauliny-Toth, I. I. K., Steppe, H., and Witzel, A. 1980, A&A, 88, L12.

Suchkov, A. A., Hanisch, R. J., Voges, W., and Heckman, T. M. 2006, AJ, 132,1475.

Sun, Y. C., Bai, Y., He, X. T., Chen, Y., et al. 2012, Progress in Astronomy, 30, 106.

Tananbaum, H., Wardle, J. F. C., Zamorani, G., and Avni, Y. 1983, APJ, 268, 60.

Traulsen, I., Schwope, A. D., Lamer, G., Ballet, J., Carrera, F., et al. 2019, A&A, 624, A77.

Urry, C. M., Padovani, P. 1995, PASP, 107, 803.

Willott, C. J., Rawlings, S., Blundell, K. M., Lacy, M., and Eales, S. A. 2001, MNRAS, 322, 536.

Worrall, D. M., Giommi, P., Tananbaum, H., and Zamorani, G. 1987, APJ, 313, 596.

York, D. G., et al. 2000, AJ, 120, 1579.

Young, M., Elvis, M., and Risaliti, G. 2009, ApJS, 183, 17.

Zhao, G. B., Crittenden, R. G., Pogosian, L., and Zhang, X. 2012, PhRvL, 109, 171301.

Zhu, S. F., Brandt, W. N., Luo, B., Wu, J., Xue, Y. Q., and Yang, G. 2020, MNRAS, 496, 245.